

A formulation of domain-wall fermions in the Schrödinger functional

Shinji Takeda*

Physics Department, Columbia University,
New York, NY 10027 USA

September 14, 2018

Abstract

We present a formulation of domain-wall fermions in the Schrödinger functional by following a universality argument. To examine the formulation, we numerically investigate the spectrum of the free operator and perform a one-loop analysis to confirm universality and renormalizability. We also study the breaking of the Ginsparg-Wilson relation to understand the structure of chiral symmetry breaking from two sources: The bulk and boundary. Furthermore, we discuss the lattice artifacts of the step scaling function by comparing with other fermion discretizations.

1 Introduction

In the study of CP violation by CKM unitary triangle analysis, hadron matrix elements of four-fermion operators, such as B_K , play a vital role. Accurate calculations of this quantity from first principles are an important task for the lattice QCD community. In such calculations, having chiral symmetry is crucial to avoid an operator mixing problem which causes uncontrollable systematic errors. Although lattice chiral fermions [1, 2, 3] are a clean formulation, they require enormous computing power to perform dynamical simulations. In comparison, ordinary fermion formulations, like Wilson type fermions and staggered

*Present address: Institute for Theoretical Physics, Kanazawa University, Kanazawa 920-1192, Japan. E-mail address: takeda@hep.s.kanazawa-u.ac.jp

fermions are relatively cheap. Nowadays, however, thanks to the development of computer architecture and algorithms, dynamical simulations with lattice chiral fermions have become feasible even for three flavors [4]. In particular, the RBC/UKQCD collaboration [5] is currently using domain-wall fermions (DWFs) to compute B_K . In the course of their computation, there are many sources of systematic errors which one has to control. Among them, the non-perturbative renormalization (NPR) could be serious. At the moment, the collaboration has been using conventional schemes, such as, the RI/MOM scheme and its variants [6, 7]. However, these schemes potentially contain “large scale problem” which requires a quite large lattice volume. To avoid such difficulties, a new scheme was invented, known as the Schrödinger functional (SF) scheme [8]. This scheme provides a reliable way of estimating errors in the NPR. If one wants to use this scheme for the renormalization of B_K given by the RBC collaboration, first of all, one has to formulate DWF in the SF setup. This is the purpose of this paper.

While chiral fermions are useful for computing the bare B_K to avoid the mixing problem, a formulation for such fermions in the SF setup was a non-trivial task because SF boundary conditions break chiral symmetry explicitly. We will address this issue in the next section. However, Taniguchi [9] made the first attempt to formulate overlap fermions by using an orbifolding technique. Subsequently he provided a formulation for domain-wall fermions and then he and his collaborators [10] calculated a renormalized B_K in quenched QCD. Sint [11] developed such techniques by combining with a flavor twisting trick. However, these orbifolding formulations are constrained by the requirement that the number of flavors be even. Thus, apparently such formulations are incompatible with current trends toward dynamical three flavor simulations. To overcome this difficulty, Lüscher [12] gave a completely different approach relying on a universality argument, dimensional power counting and symmetry considerations. Some perturbative calculations were performed in Ref. [13]. A crucial property of this formulation is that there is no restriction on the number of flavors. Since only overlap fermions were considered in Ref. [12], our main purpose here is to formulate the other chiral fermions, namely, domain-wall fermions.

The rest of the paper is organized as follows. Section 2 gives the formulation of domain-wall fermions in the SF setup, after a brief review of the universality argument. We present several pieces of numerical evidence in Section 3 and 4 to show that our formulation is working properly. We also discuss the lattice artifacts for the step scaling function in Section 5. In the last section, we conclude by giving some remarks and outlook.

2 Formulation

In the following, we assume that the reader is familiar with the SF in QCD [8, 14]. After giving a brief reminder of the universality argument, we give a formulation for DWF and finally check the chiral symmetry breaking structure numerically.

2.1 Universality argument

In the massless continuum theory, the Dirac operator D satisfies the anti-commutation relation with γ_5

$$\gamma_5 D + D \gamma_5 = 0. \quad (1)$$

The above is true even in the SF setup, although the boundary conditions,

$$P_+ \psi(x) = 0 \quad \text{at} \quad x_0 = 0, \quad (2)$$

$$P_- \psi(x) = 0 \quad \text{at} \quad x_0 = T, \quad (3)$$

with $P_\pm = (1 \pm \gamma_0)/2$, break chiral symmetry explicitly. Eq.(1) means that the operator itself does not know about boundary conditions. In the continuum theory, information such as boundary conditions is embedded in the Hilbert space. In fact, the corresponding propagator, which is a solution of the inhomogeneous equation,

$$DS(x, y) = \delta(x - y), \quad (4)$$

fails to satisfy the anti-commutation relation. Instead, it follows

$$\begin{aligned} \gamma_5 S(x, y) + S(x, y) \gamma_5 = \\ \int_{z_0=0} d^3 \mathbf{z} S(x, z) \gamma_5 P_- S(z, y) + \int_{z_0=T} d^3 \mathbf{z} S(x, z) \gamma_5 P_+ S(z, y). \end{aligned} \quad (5)$$

This can be derived by using partial integration on the SF manifold which has two boundaries at time slice $x_0 = 0$ and T . The non-vanishing right-hand side in eq.(5) shows an explicit chiral symmetry breaking. Since such a breaking term is supported only on the time boundaries, the chiral symmetry is preserved in a bulk.

If someone naively tries to formulate chiral fermions on the lattice, one may define an overlap operator, for example, with the Wilson kernel in the SF setup [14]. However such an operator immediately satisfies the Ginsberg-Wilson relation and thus cannot reproduce eq.(5) in the continuum limit. This indicates that such naive formulation does not work and furthermore may belong to another boundary universality class which is not what we want. In this way, it is a non-trivial task to formulate chiral fermions in the SF setup.

Some years ago, Lüscher [12] proposed a clever way to overcome this situation. First, consider the relation for the propagator in eq.(5). This indicates

that the GW relation has to be modified by boundary effects. Thus one has to find a modified overlap operator which breaks the GW relation near the time boundaries and correctly reproduces eq.(5) in the continuum limit. Actually, finding such a modified operator is not so hard. However, a new question naturally arising is how the SF boundary conditions emerge. For the Wilson fermion case [14], because there is a transfer matrix, it is natural for fermion fields to follow the SF boundary conditions. However for chiral fermions, there is no such transfer matrix which can be defined from nearest neighbor interaction in the time direction. Therefore it is not an easy task.

Lüscher [12] gave another point of view to see how fields respect the boundary condition. In the quantum field theory, the correlation function can tell you what kinds of boundary conditions are imposed. As an example, let us see how the boundary conditions emerge for Wilson fermions whose action is given by

$$S_w = \sum_x \bar{\psi}(x) D_w(m) \psi(x), \quad (6)$$

$$D_w(m) = \frac{1}{2} \left[\sum_{\mu} (\nabla_{\mu} + \nabla_{\mu}^*) \gamma_{\mu} - a \sum_{\mu} \nabla_{\mu}^* \nabla_{\mu} \right] + m, \quad (7)$$

where ∇_{μ} and ∇_{μ}^* are forward and backward covariant difference operators respectively,

$$\nabla_{\mu} \psi(x) = \frac{1}{a} [U(x, \mu) \psi(x + a\hat{\mu}) - \psi(x)], \quad (8)$$

$$\nabla_{\mu}^* \psi(x) = \frac{1}{a} [\psi(x) - U(x - a\hat{\mu}, \mu)^{-1} \psi(x - a\hat{\mu})]. \quad (9)$$

In the SF setup, the sum over x in the action is a little bit subtle. We assume that the dynamical fields are $\psi(x)$ with $a \leq x_0 \leq T - a$ and the fields $\psi(x)$ with $x_0 \leq 0$ and $T \leq x_0$ are set to zero. For this setup, the propagator may be defined by

$$\langle \eta(x) \bar{\psi}(y) \rangle = a^{-4} \delta_{x,y}, \quad (10)$$

$$\eta(x) = \frac{\delta S_w}{\delta \bar{\psi}(x)}. \quad (11)$$

For $2a \leq x_0 \leq T - 2a$, eq.(11) turns out to be

$$\eta(x) = D_w(m) \psi(x). \quad (12)$$

On the other hand, at $x_0 = a$, we obtain

$$\begin{aligned} \eta(x) &= \frac{1}{a} P_+ \psi(x) - \nabla_0 P_- \psi(x) \\ &+ \frac{1}{2} \left[\sum_k (\nabla_k + \nabla_k^*) \gamma_k - a \sum_k \nabla_k^* \nabla_k \right] \psi(x) + m \psi(x). \end{aligned} \quad (13)$$

By substituting eq.(13) into eq.(10) with $x \neq y$ we obtain

$$\frac{1}{a}P_+\langle\psi(x)\bar{\psi}(y)\rangle|_{x_0=a} - \nabla_0 P_-\langle\psi(x)\bar{\psi}(y)\rangle|_{x_0=a} + \dots = 0. \quad (14)$$

In the continuum limit, the first term is dominant

$$\frac{1}{a}P_+\langle\psi(x)\bar{\psi}(y)\rangle|_{x_0=0} = 0. \quad (15)$$

This shows that in the naive continuum limit, the Dirichlet type boundary condition ($P_+\psi|_{x_0=0} = 0$) is stable against the Neumann one ($\nabla_0 P_-\psi|_{x_0=0} = 0$), and in the end the SF boundary conditions in eq.(2) emerge. It is plausible that similar things happen also for the chiral fermions case, as long as the locality and symmetry are kept in a proper way, although we expect that the coefficient of the lowest dimensional operators ($\frac{1}{a}P_+\psi$) may be different from the above case, and more higher dimensional terms may appear in eq.(13). The important point here is that continuum SF boundary conditions emerge dynamically in the continuum limit of the correlation function. This boundary condition is natural and automatically guaranteed to emerge from the dimensional order counting argument. Therefore, when we construct chiral fermions in the SF, we only have to prepare a modified operator by introducing an additional term which breaks the chiral symmetry near the time boundaries. Once this is fulfilled, then such an operator automatically turns out to be the desired one in the continuum limit without fine tuning. A final important note is that the form of the boundary term is irrelevant as long as it will go into a preferred boundary universality class. Therefore, there is a large amount of freedom when choosing boundary terms and one can use this freedom for practical purposes.

Following these guiding principles, Lüscher [12] proposed the operator:

$$\bar{a}D_N = 1 - \frac{1}{2}(U + \tilde{U}), \quad (16)$$

$$U = A(A^\dagger A + caP)^{-1/2}, \quad \tilde{U} = \gamma_5 U^\dagger \gamma_5, \quad (17)$$

$$A = 1 + s - aD_w(0), \quad \bar{a} = a/(1 + s), \quad (18)$$

with the parameter in the range $|s| < 1$. $D_w(0)$ is the massless Wilson operator in the SF. The key point here is the presence of the P term in the inverse square root which is given by

$$aP(x, y) = \delta_{\mathbf{x}, \mathbf{y}} \delta_{x_0, y_0} (\delta_{x_0, a} P_- + \delta_{x_0, T-a} P_+). \quad (19)$$

Note that this term is supported near the time boundaries and thus called a boundary operator. The presence of this term breaks the GW relation explicitly and the breaking is given by

$$\Delta_B = \gamma_5 D_N + D_N \gamma_5 - \bar{a} D_N \gamma_5 D_N. \quad (20)$$

It was shown in ref. [12] that this term is local and supported in the vicinity of the boundaries up to the exponentially small tails.

Although this operator breaks chiral symmetry explicitly, other symmetries (the discrete rotational symmetries, C , P and T , flavor symmetry and so on) have to be maintained since the boundary conditions in eq.(2,3) are invariant under these symmetries. In addition, this operator has γ_5 -Hermiticity. In this way, the universality formulation can avoid breaking important symmetries, such as the flavor symmetry. This is a distinctive feature of this formulation compared with the orbifolding technique, where flavor symmetries cannot be maintained or, there is a constraint on the number of flavors.

Before leaving this subsection, let us summarize the guiding principles of formulating chiral fermions in the SF setup. What we learned from this construction is that, for an original chiral fermion operator, one has to introduce an additional term to break the chiral symmetry and then demand that such breaking only appears near the time boundaries. Furthermore, one must maintain important symmetries as well as γ_5 -Hermiticity. Once these conditions are fulfilled, it is automatically guaranteed that such a lattice operator will correctly reproduce the continuum results according to the universality argument.

2.2 Formulation of domain-wall fermions

Let us apply the guiding principles given in the previous subsection to domain-wall fermions. We propose a massless¹ domain-wall fermion action

$$S = a^4 \sum_{x,x'} \sum_{s,s'=1}^{L_s} \bar{\psi}(x,s) (D_{\text{DWF}})_{xs,x's'} \psi(x',s'), \quad (21)$$

where a massless operator with $L_s = 6$ for example² in four dimensional block form is given by

$$aD_{\text{DWF}} = \begin{bmatrix} a\tilde{D}_w & -P_L & 0 & 0 & 0 & cB \\ -P_R & a\tilde{D}_w & -P_L & 0 & cB & 0 \\ 0 & -P_R & a\tilde{D}_w & -P_L + cB & 0 & 0 \\ 0 & 0 & -P_R - cB & a\tilde{D}_w & -P_L & 0 \\ 0 & -cB & 0 & -P_R & a\tilde{D}_w & -P_L \\ -cB & 0 & 0 & 0 & -P_R & a\tilde{D}_w \end{bmatrix}, \quad (22)$$

with the chiral projections,

$$P_{R/L} = (1 \pm \gamma_5)/2. \quad (23)$$

¹The mass term can be introduced in the usual way, namely $a^4 m_f \sum_{\mathbf{x}} \sum_{x_0=a}^{T-a} [\bar{\psi}(x,1) P_R \psi(x, L_s) + \bar{\psi}(x, L_s) P_L \psi(x, 1)]$.

²We restrict ourselves to an even number of L_s , which is the case usually implemented.

We also assume that the dynamical fields are $\psi(x, s)$ with $a \leq x_0 \leq T - a$. The block elements in eq.(22) are four dimensional operators and $a\tilde{D}_w$ is given by

$$a\tilde{D}_w = aD_w(-m_5) + 1. \quad (24)$$

The domain-wall height parameter usually takes a value in a range $0 < am_5 < 2$.

An important ingredient here is the presence of B in eq.(22) terms in the cross diagonal elements. The reason for this s -dependence is to break the chiral symmetry in a similar way to the usual mass term [15]. As mentioned before, such chiral symmetry breaking should be present only near time boundaries, therefore, we chose the B term as

$$B(x, y) = \delta_{\mathbf{x}, \mathbf{y}} \delta_{x_0, y_0} \gamma_5 (\delta_{x_0, a} P_- + \delta_{x_0, T-a} P_+), \quad (25)$$

which is supported near the boundaries. In this way, the time dependence is fixed. The spinor structure ($\gamma_5 P_{\pm}$) is determined by imposing the discrete symmetries C, P and T and Γ_5 -Hermiticity. These requirements are not so strong to determine the spinor structure completely and therefore there is some freedom. The structure proposed here is only one of many solutions. Actually, we examined several choices of the spinor structure in the boundary term and confirmed numerically the universal results in the continuum limit for the lowest eigenvalue. In the following, we take this boundary term in eq.(25).

The boundary coefficient c is supposed to be non-zero to correctly reproduce the continuum theory as we will see in Section 3. It also plays an important role to cancel boundary $O(a)$ cutoff effects and has a perturbative expansion

$$c = c^{(0)} + c^{(1)} g_0^2 + O(g_0^4). \quad (26)$$

In the same way as in [13], we tune the first coefficient $c^{(0)}$ as a function of the domain-wall height am_5 ,

$$\begin{aligned} c^{(0)} = & 0.5089 - 0.0067(am_5 - 1) + 0.0488(am_5 - 1)^2 \\ & - 0.0216(am_5 - 1)^3 + 0.0673(am_5 - 1)^4. \end{aligned} \quad (27)$$

This is valid in the region where bulk $O(a)$ can be neglected³, that is, for sufficient large L_s . In the process of this determination, one needs to define the operators of the axial vector current and pseudo scalar density. We give their definition together with that of the conserved axial current in appendix A.3.

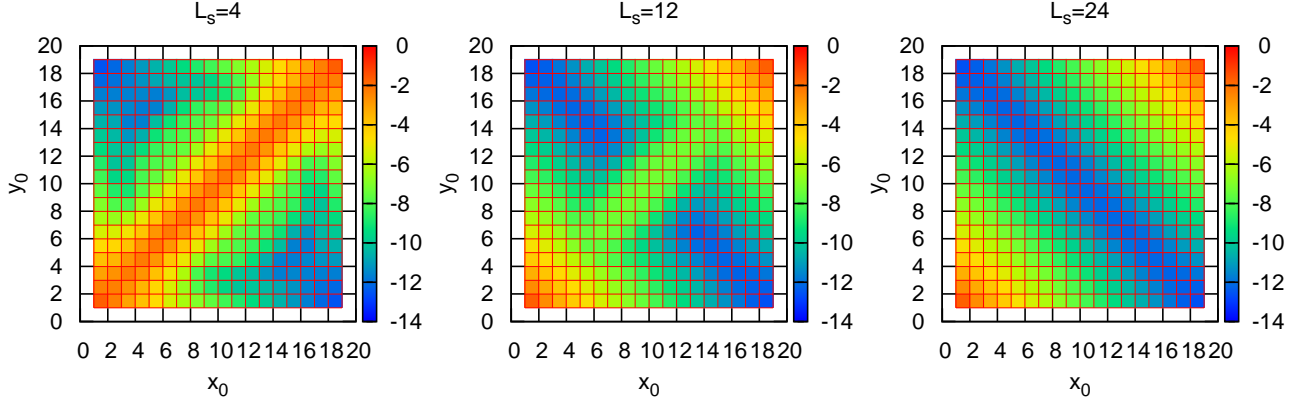


Figure 1: The color ranging $[-14, 0]$ corresponds to the value of $\ln \|\Delta^{(L_s)}(x_0, y_0)\|_{\text{spin}}$ for the zero spatial momentum configuration with the parameters $T/a = 20$, $m_f = 0$, $am_5 = 1$ and $c = 1$.

2.3 Structure of chiral symmetry breaking at tree level

In this subsection, let us check an important properties of the operator defined in the previous section. A reader may worry that even though the additional boundary term is localized to time boundary, after integrating over the fifth dimensional degree of freedom such breaking effects may leak into the 4-dim bulk and ruin the bulk chiral symmetry. To settle this question, we numerically investigate the structure of the chiral symmetry breaking by looking at the breaking of the GW relation

$$\Delta^{(L_s)} = \gamma_5 D_{\text{eff}}^{(L_s)} + D_{\text{eff}}^{(L_s)} \gamma_5 - 2a D_{\text{eff}}^{(L_s)} \gamma_5 D_{\text{eff}}^{(L_s)}, \quad (28)$$

with the effective four dimensional operator [16, 17]

$$\det D_{\text{eff}}^{(L_s)} = \det[D_{\text{DWF}}/D_{\text{PV}}]. \quad (29)$$

The Pauli-Villars (PV) operator is defined as the massive DWF operator with $am_f = -1$. To obtain the effective operator, first of all, we have to define physical

³ Actually, we observe that $O(a)$ improvement program does not work for small L_s and values of am_5 which are far from 1. For example $O(a)$ terms in f_A and f_P (defined in appendix A.3) at tree level do not vanish simultaneously with the same value of $c^{(0)}$.

quark fields

$$q(x) = P_L \psi(x, 1) + P_R \psi(x, L_s), \quad (30)$$

$$\bar{q}(x) = \bar{\psi}(x, 1)P_R + \bar{\psi}(x, L_s)P_L. \quad (31)$$

In terms of the propagator of domain-wall fermions defined from

$$D_{\text{DWF}} S_{\text{DWF}}(x, y; s, t) = a^{-4} \delta_{x,y} \delta_{s,t}, \quad (32)$$

that of the physical field is expressed

$$\begin{aligned} [q(x)\bar{q}(y)]_{\text{F}} &= S_{\text{q}}(x, y) \\ &= P_L S_{\text{DWF}}(x, y; 1, L_s) P_L + P_L S_{\text{DWF}}(x, y; 1, 1) P_R \\ &+ P_R S_{\text{DWF}}(x, y; L_s, L_s) P_L + P_R S_{\text{DWF}}(x, y; L_s, 1) P_R. \end{aligned} \quad (33)$$

In terms of S_{q} the effective operator is given by

$$aD_{\text{eff}}^{(L_s)} = (1 + a^3 S_{\text{q}})^{-1}. \quad (34)$$

In the SF setup, $\Delta^{(L_s)}$ in eq.(28) contains not only the bulk chiral symmetry breaking but also the boundary breaking. The former is supposed to be removed by taking L_s to infinity. In such limit, boundary breaking effects remain and they are expected to be localized near time boundaries. To see this situation, we numerically compute $\Delta^{(L_s)}$ for a free operator. In the free case, we can perform the Fourier transformation for spatial directions. We study the momentum configuration $\mathbf{p} = (0, 0, 0)$ in the following. The remaining dimensions are only the time direction and spinor space, therefore for a given L_s and the fixed spatial momentum configuration, $\Delta^{(L_s)}$ is a matrix with dimension $4(T/a - 1)$. Figure 1 shows the magnitude of $\ln(\|\Delta^{(L_s)}(x_0, y_0)\|_{\text{spin}})$, where the norm is taken for the spinor space only. By increasing L_s , the bulk symmetry breaking is reduced. Finally at $L_s = 24$, only boundary breaking effects remain and they are localized exponentially near the time boundaries. This is the expected behavior for overlap fermions [12]. We conclude that the presence of the boundary term causes chiral symmetry breaking, which decays exponentially away from the time boundaries for the effective four dimensional operator.

3 Spectrum of free operator

In this section, we investigate the free spectrum of the DWF operator to confirm universality at the tree level. We set $T = L$ in this section.

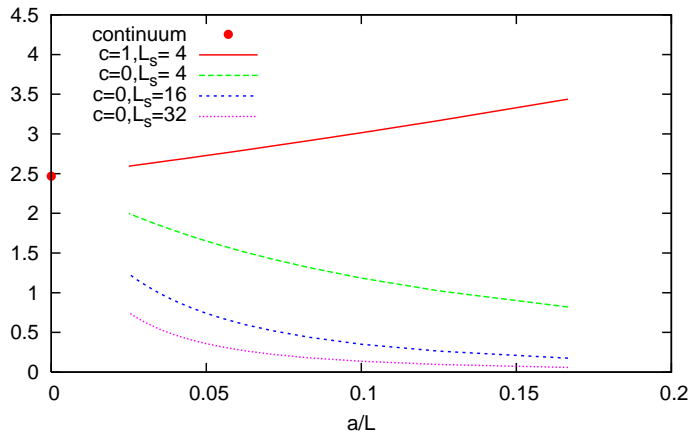


Figure 2: The lowest eigenvalue of $L^2 D_{\text{DWF}}^\dagger D_{\text{DWF}}$ with $am_5 = 1$. Some combinations of parameters c and L_s are shown. The continuum value is $\pi^2/4 = 2.467\dots$. For $c = 1$ case, since the L_s -dependence is so weak on this scale, we show only $L_s = 4$ results as representative.

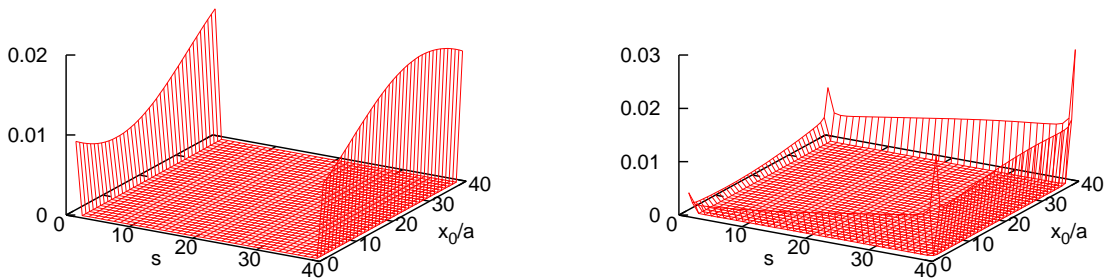


Figure 3: $\|\psi(x_0, s)\|_{\text{spin}}$ with zero spatial momentum and the parameters $T/a = L_s = 40$, $\theta = 0$ and $am_5 = 1$. The norm for the eigenvector is taken in the spinor space. The left (right) panel is for $c = 1$ ($c = 0$).

3.1 Spectrum of $D_{\text{DWF}}^\dagger D_{\text{DWF}}$

To achieve better chiral symmetry, the (physical) eigenmodes of the domain-wall operator should be localized near the boundaries of the fifth direction and propagate in the space-time directions. This should also be true in the SF setup,

since the chiral symmetry is supposed to be maintained in the bulk. To observe such phenomena, we numerically compute the lowest eigenmode of the operator $D_{\text{DWF}}^\dagger D_{\text{DWF}}$ with the trivial gauge configuration $U(x, \mu) = 1$. In the free case, we can perform the Fourier transformation for spatial directions, and project out the momentum configuration $\mathbf{p} = (0, 0, 0)$. Thus, remaining indexes of the vector space are now the spinor, the time x_0 and the extra dimension s ,

$$D_{\text{DWF}}^\dagger D_{\text{DWF}} \psi(x_0, s) = \lambda \psi(x_0, s), \quad (35)$$

where the spinor indexes are suppressed. We set input parameters $am_5 = 1$ and $\theta = 0$. θ is the parameter which controls the spatial boundary condition for fermion fields. (For more details, we refer to [18].)

We numerically compute the lowest eigenvalue and the corresponding eigenfunction $\|\psi(x_0, s)\|_{\text{spin}}$. We examine not only for $c = 1$ but also for $c = 0$ to investigate the importance of the presence of the boundary operator. The scaling behavior of the eigenvalue is shown in Figure 2. For $c = 1$, L_s dependence is too small to see on this scale. The lowest eigenvalues converge to their continuum values properly, therefore universality is confirmed. Furthermore, the associated eigenfunction shows nice localization behavior, namely being localizing for the fifth direction and propagating for the time direction, as shown in the left panel of Figure 3. This shows that this mode is a physical one.

For $c = 0$ in Figure 2, although all $L_s = 4, 16, 32$ results tend to converge to the continuum limit, large L_s results have a bending phenomenon in small a/L region and show no power decay in terms of a/L . This indicates that if one takes L_s to infinite before taking $a/L = 0$ limit, the eigenvalue will likely converge to zero. If this is so, the theory with $L_s = \infty$ does not belong to a correct universality class. Furthermore, the eigenfunction in the right panel in Figure 3 is localized on edges in the time- s plane. This is a typical unphysical mode. On the other hand, interestingly for small L_s , the scaling behavior is rather mild. In the small L_s case, the chiral symmetry breaking of domain-wall fermions are rather similar to that of the ordinary Wilson fermions. As in the Wilson fermions case, the bulk chiral symmetry breaking for DWFs due to finite L_s plays some role in producing the correct continuum limit. This is the reason why DWFs with smaller L_s and no boundary term B can produce the continuum results.

The results shown in this subsection show that the boundary term with $c \neq 0$ plays an important role for the theory to be in the correct universality class.

3.2 Spectrum of $D_{\text{q}}^\dagger D_{\text{q}}$

Not all eigenmodes of D_{DWF} are physical ones and elimination of unphysical mode is not clear. To extract physical modes only, let us study the eigenmodes

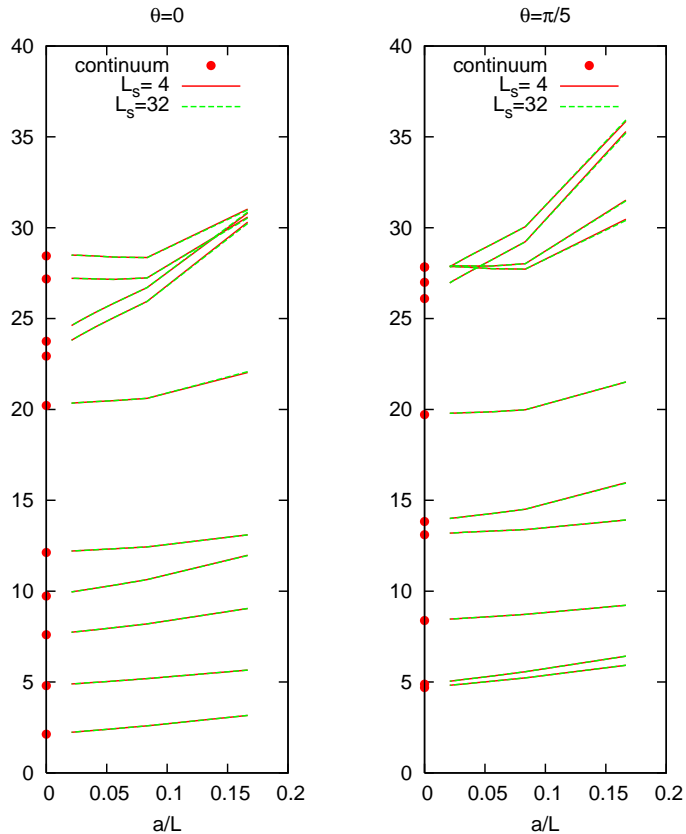


Figure 4: The a/L dependence of the lowest ten eigenvalues of $L^2 D_q^\dagger D_q$ in the presence of the background gauge field. The left (right) panel is for $\theta = 0$ ($\theta = \pi/5$). The parameters are set to $am_5 = 1$ and $c = 1$. The red points at $a/L = 0$ are continuum values [18].

of D_q , where unphysical modes are excluded. The operator D_q is defined from S_q in eq.(33)

$$D_q S_q(x, y) = a^{-4} \delta_{x, y}. \quad (36)$$

We numerically compute the lowest ten eigenvalues of $D_q^\dagger D_q$ with the parameter set $am_5 = 1$, $\theta = 0, \pi/5$ and $c = 1$ in the presence of the the background gauge field (choice A in Ref. [19]). The values obtained for $L/a = T/a = 6, 12, 24$ are summarized in Table 1. All tables are given in appendix B The scaling behavior of the eigenvalues are shown in Figure 4. Although we show two cases of L_s , namely $L_s = 4$ and $L_s = 32$, it is hard to see the difference on this scale. We observe that they converge to the continuum values given in Ref [18].

This behavior persists for a variety of values of c , $0.5 \leq c \leq 1.5$. This confirms universality at the tree level.

4 One-loop analysis of SF coupling

To check further universality at the quantum level and renormalizability, we perform the one-loop order calculation of the SF coupling.

4.1 Definition and results

We compute the fermion contribution to the SF coupling [18] $p_{1,1}(L/a, L_s)$ (we set $L = T$ as usual) at one-loop order for massless domain-wall fermions. The one-loop coefficient is given as

$$p_{1,1}(L/a, L_s) = \frac{1}{k} \frac{\partial}{\partial \eta} \ln \det(D_{\text{DWF}}/D_{\text{PV}}) \Big|_{\eta=\nu=0}, \quad (37)$$

with a normalization (See [18] for details.)

$$k = 12(L/a)^2 [\sin(\gamma) + \sin(2\gamma)], \quad \gamma = \frac{1}{3}\pi(a/L)^2. \quad (38)$$

The parameters η and ν parameterize the background gauge field [19]. In the actual calculation, we expand the η derivative and use the fact that the determinant is factorized for individual spatial momentum \mathbf{p} and color sector b ,

$$\begin{aligned} p_{1,1}(L/a, L_s) &= \frac{1}{k} \text{Tr} \left[D_{\text{DWF}}^{-1} \frac{\partial D_{\text{DWF}}}{\partial \eta} - D_{\text{PV}}^{-1} \frac{\partial D_{\text{PV}}}{\partial \eta} \right] \\ &= \frac{1}{k} \sum_{\mathbf{p}} \sum_{b=1}^3 \text{tr} \left[(D_{\text{DWF}}^b)^{-1}(\mathbf{p}) \frac{\partial D_{\text{DWF}}^b(\mathbf{p})}{\partial \eta} \right. \\ &\quad \left. - (D_{\text{PV}}^b)^{-1}(\mathbf{p}) \frac{\partial D_{\text{PV}}^b(\mathbf{p})}{\partial \eta} \right]. \end{aligned} \quad (39)$$

The trace tr concerns the spinor, the time indices and fifth coordinate only. It is maybe worthwhile to note that for our definition of DWF,

$$\frac{\partial D_{\text{DWF}}}{\partial \eta} = \frac{\partial D_{\text{PV}}}{\partial \eta} \quad (40)$$

holds since the mass term does not involve the gauge field.

We compute $p_{1,1}$ on the lattices of size $L/a = 4, 6, \dots, 48$ and $L_s = 6, 8, 10, 12, 16$ with parameters $0.7 \leq am_5 \leq 1.3$ and $\theta = \pi/5$. Subsets of the results are summarized in Table 2 for $am_5 = 1$, $L_s = 6$ and $L/a = 4, 6, \dots, 48$. Separate contributions from DWF and PV are also shown there.

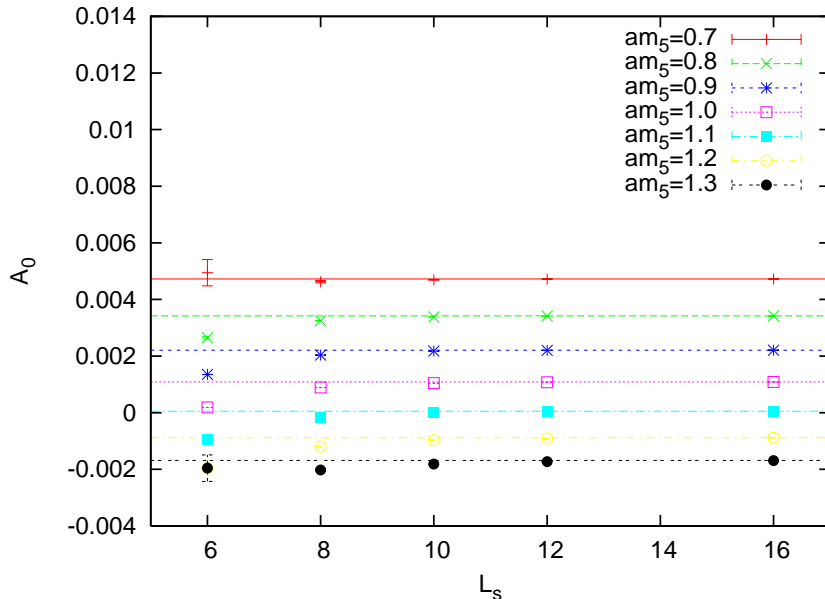


Figure 5: L_s -dependence of A_0 for $0.7 \leq am_5 \leq 1.3$. The horizontal lines show the values of A_0 in the infinity L_s limit, which are obtained by combining the results of previous literature [18, 20].

4.2 Coefficients of Symanzik's expansion

From the Symanzik's analysis of the cutoff dependence of Feynman diagrams on the lattice, one expects that the one-loop coefficient has an asymptotic expansion in terms of a/L

$$p_{1,1}(L/a, L_s) = \sum_{n=0}^{\infty} (a/L)^n [A_n(L_s) + B_n(L_s) \ln(L/a)]. \quad (41)$$

Note that the coefficients A_n and B_n ($n = 0, 1, 2, \dots$) depend on L_s . We can reliably extract the first few coefficients by making use of the method described in Ref. [21].

For the usual renormalization of the coupling constant, B_0 at $L_s = \infty$ should be $2b_{0,1}$ where $b_{0,1}$ is the fermion part of the one-loop coefficient of the β -function

for N_f flavors QCD,

$$b_0 = b_{0,0} + N_f b_{0,1}, \quad (42)$$

$$b_{0,0} = \frac{11}{(4\pi)^2}, \quad (43)$$

$$b_{0,1} = -\frac{2}{3} \frac{1}{(4\pi)^2}. \quad (44)$$

We confirmed that $B_0(L_s)$ for large L_s (say $L_s = 16$) converges to $2b_{0,1} = -0.008443\dots$ up to three significant digits for the values of am_5 which we investigated. When the tree-level $O(a)$ improvement is realized, we expect that $B_1 = 0$ holds. We check this to 10^{-3} for the same parameter region as before. This shows that the formula for the boundary coefficient in eq.(27) works well to achieve the tree-level $O(a)$ improvement to the precision considered here. In the following analysis, we set exact values $B_0 = 2b_{0,1} = -1/(12\pi^2)$ and $B_1 = 0$.

A_0 gives information about a ratio of Λ -parameters. The obtained values of $A_0(L_s)$ as a function of L_s are shown in Figure 5. By combining the previous results from Ref. [18, 20], the values of A_0 at infinity L_s can be obtained, and are shown in Figure 5 as the horizontal lines. We observe that our results at finite L_s properly converge to the known results at infinity L_s .

To achieve one-loop $O(a)$ improvement, we need to determine the coefficient of the fermion part of the boundary counter-term, $c_t^{(1,1)}$ [18] at one-loop order. If one imposes an improvement condition [18], one finds that

$$c_t^{(1,1)} = A_1/2, \quad (45)$$

therefore we need the value of A_1 . The obtained values of A_1 are given in Table 3. For future reference, we provide an interpolation formula for $c_t^{(1,1)}$ as a polynomial of am_5 for larger L_s , where value of A_1 is saturated,

$$c_t^{(1,1)} = 0.00434 + 0.01102(am_5 - 1) - 0.00858(am_5 - 1)^2, \quad (46)$$

for $0.7 \leq am_5 \leq 1.3$.

5 Lattice artifacts of the step scaling function to one-loop order

In this section, we investigate lattice artifacts of the step scaling function (SSF) [22] $\sigma(2, u)$, which describes the evolution of the running coupling $\bar{g}^2(L) = u$ under changes of scale L by a factor 2,

$$\sigma(2, u) = \bar{g}^2(2L), \quad u = \bar{g}^2(L). \quad (47)$$

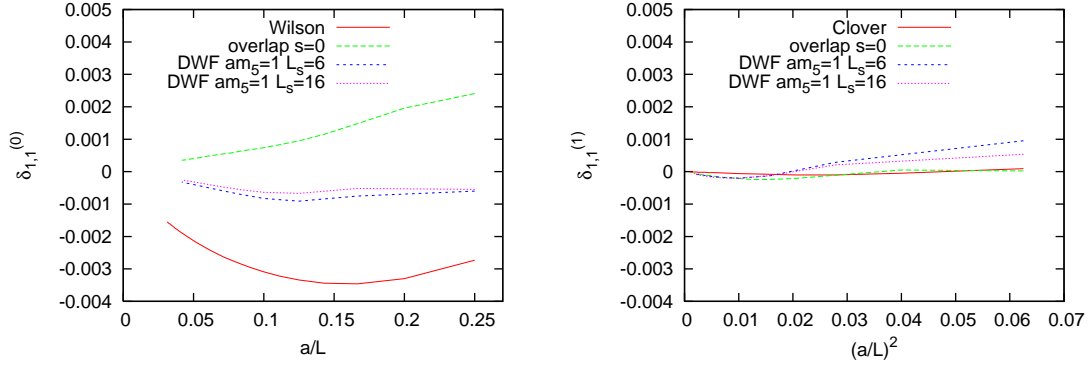


Figure 6: We show the relative deviation with the various actions for tree level $O(a)$ improvement, $\delta_{1,1}^{(0)}$ (Left), and one-loop $O(a)$ improvement, $\delta_{1,1}^{(1)}$ (Right), as a function of a/L and $(a/L)^2$ respectively. Upper part is for $\theta = 0$, and lower is for $\theta = \pi/5$. For comparison, those of the Wilson type fermion with $c_t^{(1,1)} = 0$ and the clover fermion with $c_t^{(1,1)} = 0.019141$ [18] are included in the plot of $\delta_{1,1}^{(0)}$ and $\delta_{1,1}^{(1)}$ respectively.

The lattice version of the step scaling function is denoted by $\Sigma(2, u, a/L)$ which contains lattice artifacts. Such lattice artifacts are described by the relative deviation

$$\delta(u, a/L) \equiv \frac{\Sigma(2, u, a/L) - \sigma(2, u)}{\sigma(2, u)}. \quad (48)$$

By expanding the relative deviation in terms of the coupling constant u , one obtains

$$\delta(u, a/L) = \delta_1(a/L)u + O(u^2), \quad (49)$$

where the one-loop deviation, $\delta_1(s, a/L)$, may be decomposed into pure gauge and fermion part [18],

$$\delta_1(a/L) = \delta_{1,0}(a/L) + N_f \delta_{1,1}(a/L). \quad (50)$$

We are currently only interested in the fermion part. We consider domain-wall fermions, thus the fermion part of the one-loop deviation $\delta_{1,1}(a/L, L_s)$ contains L_s dependence. In terms of the one-loop coefficient of the SF coupling $p_{1,1}$, the one-loop deviation is given by

$$\delta_{1,1}(a/L, L_s) = p_{1,1}(2L/a, L_s) - p_{1,1}(L/a, L_s) - 2b_{0,1} \ln(2). \quad (51)$$

Depending on the value of the boundary counter term $c_t^{(1,1)}$, we denote with $\delta_{1,1}^{(0)}$ the tree level $O(a)$ improved version with $c_t^{(1,1)} = 0$, and $\delta_{1,1}^{(1)}$ the one-loop $O(a)$ improved one for $c_t^{(1,1)}$ in eq.(45).

We show numerical results for the one-loop deviation in Tables 4 and 5 and the plots in Figure 6, where we include those of the Wilson type fermions [18] and overlap fermion [13] for comparison. L_s -dependence of DWFs is small. In the case of the clover action, $c_t^{(1,1)}$ is set to be the proper value to achieve one-loop $O(a)$ improvement, and for Wilson fermions it is set to $c_t^{(1,1)} = 0$. We observe that the lattice artifacts for domain-wall fermions are small for tree level boundary $O(a)$ improvement case compared with other fermions, while they are large for one-loop boundary $O(a)$ improvement case.

6 Conclusion and outlook

In this paper, we provide a new formulation of domain-wall fermions in the SF setup by following the universality argument of Lüscher. In contrast to the previous formulation by Taniguchi, ours can deal with the boundary $O(a)$ improvement properly, and there is no constraint on the number of flavors. To check that our formulation works properly, we investigate the spectrum and eigenmodes of the free operator, and perform a one-loop analysis of the SF coupling constant. Then we confirm universality at tree and the one-loop level and observe that all results investigated show the desired behaviors.

Before starting simulations, the boundary improvement coefficient c should be determined to one-loop order. This involves calculations of the SF correlators, f_A , f_P etc. given in appendix A. This could be done in a similar way to the case of the Wilson fermion.

As mentioned before, one of the most important properties of the universality formulation is that there are no restriction of the number of flavors. By taking advantage of this property, we may compute the renormalization factor of B_K for $N_f = 3$ QCD.

Acknowledgments

We would like to thank Sinya Aoki, Yasumichi Aoki, Norman Christ, Michael Endres, Taku Izubuchi, Changhoan Kim, Robert Mawhinney and the members of the RBC Collaboration for helpful discussions. We are grateful to Stefan Sint for his hospitality during our stay at Trinity College in Dublin, where this work was initiated. This work is supported by the U.S. Department of Energy under Grant No. DE-FG02-92ER40699.

A Fermion correlators

In this appendix, I summarize fermion correlators, the boundary fields and so on which are often used in the SF setup.

A.1 Boundary fields

As given in Ref. [12], the lattice version of the fermion boundary fields are defined

$$\zeta(\mathbf{x}) = U(x - a\hat{0}, 0)P_-q(x)|_{x_0=a}, \quad (52)$$

$$\bar{\zeta}(\mathbf{x}) = \bar{q}(x)P_+U(x - a\hat{0}, 0)^{-1}|_{x_0=a}, \quad (53)$$

$$\zeta'(\mathbf{x}) = U(x, 0)^{-1}P_+q(x)|_{x_0=T-a}, \quad (54)$$

$$\bar{\zeta}'(\mathbf{x}) = \bar{q}(x)P_-U(x, 0)|_{x_0=T-a}. \quad (55)$$

Here note that we use the physical quark fields defined in eq.(30) and (31).

A.2 Propagators

The propagators for the physical quark fields and the boundary fields are given by

$$[q(x)\bar{q}(y)]_F = S_q(x, y), \quad (56)$$

$$[q(x)\bar{\zeta}(\mathbf{y})]_F = S_q(x, y)U(y - a\hat{0}, 0)^{-1}P_+|_{y_0=a}, \quad (57)$$

$$[q(x)\bar{\zeta}'(\mathbf{y})]_F = S_q(x, y)U(y, 0)P_-|_{y_0=T-a}, \quad (58)$$

$$[\zeta(\mathbf{x})\bar{q}(y)]_F = P_-U(x - a\hat{0}, 0)S_q(x, y)|_{x_0=a}, \quad (59)$$

$$[\zeta'(\mathbf{x})\bar{q}(y)]_F = P_+U(x, 0)^{-1}S_q(x, y)|_{x_0=T-a}, \quad (60)$$

$$[\zeta(\mathbf{x})\bar{\zeta}'(\mathbf{y})]_F = P_-U(x - a\hat{0}, 0)S_q(x, y)U(y, 0)P_-|_{x_0=a, y_0=T-a}, \quad (61)$$

$$[\zeta'(\mathbf{x})\bar{\zeta}(\mathbf{y})]_F = P_+U(x, 0)^{-1}S_q(x, y)U(y - a\hat{0}, 0)^{-1}P_-|_{x_0=T-a, y_0=a}. \quad (62)$$

A.3 Operators

We consider the degenerate quark mass case and an extension of the flavor space is done in a trivial way. In terms of the physical quark fields, the local operators are defined as

$$A_\mu^a(x) = \bar{q}(x)\gamma_\mu\gamma_5\frac{1}{2}\tau^a q(x), \quad (63)$$

$$P^a(x) = \bar{q}(x)\gamma_5\frac{1}{2}\tau^a q(x). \quad (64)$$

The conserved axial vector current is given by

$$\mathcal{A}_\mu^a(x) = \sum_{s=1}^{L_s} \text{sign} \left(s - \frac{L_s + 1}{2} \right) j_\mu^a(x, s), \quad (65)$$

where

$$\begin{aligned} j_\mu^a(x, s) &= \bar{\psi}(x + a\hat{\mu}, s) P_+^{(\mu)} U(x, \mu)^{-1} \frac{1}{2} \tau^a \psi(x, s) \\ &\quad - \bar{\psi}(x, s) P_-^{(\mu)} U(x, \mu) \frac{1}{2} \tau^a \psi(x + a\hat{\mu}, s), \end{aligned} \quad (66)$$

with $P_\pm^{(\mu)} = (1 \pm \gamma_\mu)/2$.

A.4 Correlators

The fermion correlators for the local operators in the SF are given by

$$f_A(x_0) = -a^6 \sum_{a=1}^{N_f} \sum_{\mathbf{y}, \mathbf{z}} \frac{1}{N_f^2 - 1} \langle A_0^a(x) \bar{\zeta}(\mathbf{y}) \gamma_5 \frac{1}{2} \tau^a \zeta(\mathbf{z}) \rangle, \quad (67)$$

$$f_P(x_0) = -a^6 \sum_{a=1}^{N_f} \sum_{\mathbf{y}, \mathbf{z}} \frac{1}{N_f^2 - 1} \langle P^a(x) \bar{\zeta}(\mathbf{y}) \gamma_5 \frac{1}{2} \tau^a \zeta(\mathbf{z}) \rangle, \quad (68)$$

$$f_1 = -\frac{a^{12}}{L^6} \sum_{a=1}^{N_f} \sum_{\mathbf{u}, \mathbf{v}, \mathbf{y}, \mathbf{z}} \frac{1}{N_f^2 - 1} \langle \bar{\zeta}'(\mathbf{u}) \gamma_5 \frac{1}{2} \tau^a \zeta'(\mathbf{v}) \bar{\zeta}(\mathbf{y}) \gamma_5 \frac{1}{2} \tau^a \zeta(\mathbf{z}) \rangle. \quad (69)$$

After Wick contraction, they become

$$f_A(x_0) = a^6 \sum_{\mathbf{y}, \mathbf{z}} \frac{1}{2} \langle [\zeta(\mathbf{z}) \bar{q}(x)]_{\text{F}} \gamma_0 \gamma_5 [q(x) \bar{\zeta}(\mathbf{y})]_{\text{F}} \gamma_5 \rangle, \quad (70)$$

$$f_P(x_0) = a^6 \sum_{\mathbf{y}, \mathbf{z}} \frac{1}{2} \langle [\zeta(\mathbf{z}) \bar{q}(x)]_{\text{F}} \gamma_5 [q(x) \bar{\zeta}(\mathbf{y})]_{\text{F}} \gamma_5 \rangle, \quad (71)$$

$$f_1 = \frac{a^{12}}{L^6} \sum_{\mathbf{u}, \mathbf{v}, \mathbf{y}, \mathbf{z}} \frac{1}{2} \langle [\zeta(\mathbf{z}) \bar{\zeta}'(\mathbf{u})]_{\text{F}} \gamma_5 [\zeta'(\mathbf{v}) \bar{\zeta}(\mathbf{y})]_{\text{F}} \gamma_5 \rangle, \quad (72)$$

where the propagators are given in subsection A.2 and we have used

$$\sum_{a=1}^{N_f} \text{tr} \left[\left(\frac{\tau^a}{2} \right)^2 \right] = \frac{N_f^2 - 1}{2}. \quad (73)$$

These correlators are the same as those of Wilson fermions except that the propagators are replaced by those of the physical quark field S_q .

For the conserved axial vector current, a correlator is given by

$$f_{\mathcal{A}}(x_0) = -a^6 \sum_{a=1}^{N_f} \sum_{\mathbf{y}, \mathbf{z}} \frac{1}{N_f^2 - 1} \langle \mathcal{A}_0^a(x) \bar{\zeta}(\mathbf{y}) \gamma_5 \frac{1}{2} \tau^a \zeta(\mathbf{z}) \rangle. \quad (74)$$

As an example, at tree level, this can be expressed in terms of the propagator for domain-wall fermions as,

$$\begin{aligned} f_{\mathcal{A}}(x_0)|_{U=1} = & \sum_{s=1}^{L_s} \text{sign}\left(s - \frac{L_s + 1}{2}\right) \frac{1}{2} \text{Tr} \left[\right. \\ & -P_+ S_{\text{DWF}}(x, y; s, 1) \gamma_0 P_L S_{\text{DWF}}(y, x + a\hat{0}; 1, s) \\ & + P_- S_{\text{DWF}}(x + a\hat{0}, y; s, 1) \gamma_0 P_L S_{\text{DWF}}(y, x; 1, s) \\ & + P_+ S_{\text{DWF}}(x, y; s, 1) P_R S_{\text{DWF}}(y, x + a\hat{0}; L_s, s) \\ & - P_- S_{\text{DWF}}(x + a\hat{0}, y; s, 1) P_R S_{\text{DWF}}(y, x; L_s, s) \\ & - P_+ S_{\text{DWF}}(x, y; s, L_s) P_L S_{\text{DWF}}(y, x + a\hat{0}; 1, s) \\ & + P_- S_{\text{DWF}}(x + a\hat{0}, y; s, L_s) P_L S_{\text{DWF}}(y, x; 1, s) \\ & + P_+ S_{\text{DWF}}(x, y; s, L_s) \gamma_0 P_R S_{\text{DWF}}(y, x + a\hat{0}; L_s, s) \\ & \left. - P_- S_{\text{DWF}}(x + a\hat{0}, y; s, L_s) \gamma_0 P_R S_{\text{DWF}}(y, x; L_s, s) \right]. \quad (75) \end{aligned}$$

B Tables of numerical results

References

- [1] D. B. Kaplan, *A method for simulating chiral fermions on the lattice*, *Phys. Lett.* **B288** (1992) 342–347 [[hep-lat/9206013](#)].
- [2] Y. Shamir, *Chiral fermions from lattice boundaries*, *Nucl. Phys.* **B406** (1993) 90–106 [[hep-lat/9303005](#)].
- [3] H. Neuberger, *Exactly massless quarks on the lattice*, *Phys. Lett.* **B417** (1998) 141–144 [[hep-lat/9707022](#)].
- [4] J. Noaki *et. al.*, *Light meson spectrum with $N_f = 2 + 1$ dynamical overlap fermions*, [0810.1360](#).
- [5] **RBC-UKQCD** Collaboration, C. Allton *et. al.*, *Physical Results from 2+1 Flavor Domain Wall QCD and $SU(2)$ Chiral Perturbation Theory*, *Phys. Rev.* **D78** (2008) 114509 [[0804.0473](#)].
- [6] Y. Aoki *et. al.*, *Non-perturbative renormalization of quark bilinear operators and B_K using domain wall fermions*, *Phys. Rev.* **D78** (2008) 054510 [[0712.1061](#)].

- [7] C. Sturm *et. al.*, *Renormalization of quark bilinear operators in a MOM-scheme with a non-exceptional subtraction point*, *Phys. Rev.* **D80** (2009) 014501 [0901.2599].
- [8] M. Lüscher, R. Narayanan, P. Weisz and U. Wolff, *The Schrödinger functional: A renormalizable probe for nonabelian gauge theories*, *Nucl. Phys.* **B384** (1992) 168–228 [hep-lat/9207009].
- [9] Y. Taniguchi, *Schrödinger functional formalism with Ginsparg-Wilson fermion*, *JHEP* **12** (2005) 037 [hep-lat/0412024].
- [10] **CP-PACS** Collaboration, Y. Nakamura, S. Aoki, Y. Taniguchi and T. Yoshie, *Precise determination of B_K and right quark masses in quenched domain-wall QCD*, *Phys. Rev.* **D78** (2008) 034502 [0803.2569].
- [11] S. Sint, *The chirally rotated Schrödinger functional with Wilson fermions and automatic $O(a)$ improvement*, 1008.4857.
- [12] M. Lüscher, *The Schrödinger functional in lattice QCD with exact chiral symmetry*, *JHEP* **05** (2006) 042 [hep-lat/0603029].
- [13] S. Takeda, *Perturbative analysis of the Neuberger-Dirac operator in the Schrödinger functional*, *Nucl. Phys.* **B796** (2008) 402–421 [0712.1469].
- [14] S. Sint, *On the Schrödinger functional in QCD*, *Nucl. Phys.* **B421** (1994) 135–158 [hep-lat/9312079].
- [15] N. H. Christ and G. Liu, *Massive domain wall fermions*, *Nucl. Phys. Proc. Suppl.* **129** (2004) 272–274.
- [16] Y. Kikukawa and T. Noguchi, *Low energy effective action of domain-wall fermion and the Ginsparg-Wilson relation*, hep-lat/9902022.
- [17] Y. Kikukawa, *Locality bound for effective four-dimensional action of domain-wall fermion*, *Nucl. Phys.* **B584** (2000) 511–527 [hep-lat/9912056].
- [18] S. Sint and R. Sommer, *The running coupling from the QCD Schrödinger functional: A one loop analysis*, *Nucl. Phys.* **B465** (1996) 71–98 [hep-lat/9508012].
- [19] M. Lüscher, R. Sommer, P. Weisz and U. Wolff, *A precise determination of the running coupling in the $SU(3)$ Yang-Mills theory*, *Nucl. Phys.* **B413** (1994) 481–502 [hep-lat/9309005].
- [20] S. Aoki and Y. Kuramashi, *The lattice Lambda parameter in domain wall QCD*, *Phys. Rev.* **D68** (2003) 034507 [hep-lat/0306008].
- [21] **ALPHA** Collaboration, A. Bode, P. Weisz and U. Wolff, *Two loop computation of the Schrödinger functional in lattice QCD*, *Nucl. Phys.* **B576** (2000) 517–539 [hep-lat/9911018].

- [22] M. Lüscher, P. Weisz and U. Wolff, *A numerical method to compute the running coupling in asymptotically free theories*, *Nucl. Phys.* **B359** (1991) 221–243.

$\theta = 0$								
n	$L/a = 6$		$L/a = 12$		$L/a = 24$		b	d
	$L_s = 4$	$L_s = 32$	$L_s = 4$	$L_s = 32$	$L_s = 4$	$L_s = 32$		
1	3.161141	3.160760	2.591269	2.591267	2.350053	2.350053	2	2
2	5.658392	5.658925	5.191148	5.191161	4.990293	4.990293	2	2
3	9.050173	9.045312	8.196497	8.196424	7.888424	7.888424	3	2
4	11.981137	11.963010	10.635061	10.634737	10.177881	10.177878	1	2
5	13.098016	13.101850	12.434736	12.434839	12.281233	12.281235	3	2
6	22.037107	22.078353	20.612026	20.613136	20.436083	20.436098	1	2
7	30.304338	30.232012	25.944369	25.942289	24.578258	24.578235	2	2
8	30.810696	30.865401	26.708727	26.709232	25.378691	25.378700	2	2
9	30.585955	30.530965	27.241272	27.239584	27.184415	27.184395	1	6
10	31.026393	30.978110	28.357563	28.355829	28.438888	28.438866	3	6
$\theta = \pi/5$								
n	$L/a = 6$		$L/a = 12$		$L/a = 24$		b	d
	$L_s = 4$	$L_s = 32$	$L_s = 4$	$L_s = 32$	$L_s = 4$	$L_s = 32$		
1	5.924559	5.922886	5.232916	5.232896	4.952553	4.952553	2	2
2	6.428276	6.423570	5.566868	5.566810	5.214696	5.214695	1	2
3	9.221621	9.223322	8.721989	8.722031	8.548948	8.548949	2	2
4	13.912656	13.926143	13.392223	13.392552	13.267533	13.267537	1	2
5	15.970852	15.951467	14.513964	14.513548	14.162258	14.162253	3	2
6	21.508691	21.520321	19.983404	19.983750	19.838031	19.838036	3	2
7	35.296282	35.214384	29.231042	29.228128	27.743584	27.743548	2	2
8	35.861910	35.932144	30.057783	30.058382	28.612335	28.612346	2	2
9	30.468452	30.406862	27.727188	27.725168	27.806412	27.806386	1	6
10	31.520474	31.475867	28.021244	28.019681	27.896264	27.896245	3	6

Table 1: The lowest ten eigenvalues of the Hermitian operator $L^2 D_q^\dagger D_q$ for $L_s = 4, 32$. Upper (Lower) panel is for $\theta = 0$ ($\theta = \pi/5$). b represents the color sector, and d is for degeneracy for one flavor.

L/a	$p_{1,1}(L/a, 6)$	DWF contribution	PV contribution
4	-0.0090558230	-0.0463742376	-0.0373184146
6	-0.0128831139	-0.0614487481	-0.0485656342
8	-0.0155107254	-0.0717039592	-0.0561932338
10	-0.0176883193	-0.0786362064	-0.0609478871
12	-0.0194881626	-0.0835634805	-0.0640753179
14	-0.0209908578	-0.0872753290	-0.0662844712
16	-0.0222708990	-0.0902037775	-0.0679328785
18	-0.0233830732	-0.0925954634	-0.0692123901
20	-0.0243655725	-0.0946007679	-0.0702351955
22	-0.0252452627	-0.0963170183	-0.0710717556
24	-0.0260415528	-0.0978103244	-0.0717687716
26	-0.0267688671	-0.0991273624	-0.0723584952
28	-0.0274382013	-0.1003021397	-0.0728639383
30	-0.0280581232	-0.1013600906	-0.0733019674
32	-0.0286354356	-0.1023206640	-0.0736852285
34	-0.0291756284	-0.1031990186	-0.0740233902
36	-0.0296831955	-0.1040071669	-0.0743239714
38	-0.0301618611	-0.1047547685	-0.0745929075
40	-0.0306147460	-0.1054496923	-0.0748349463
42	-0.0310444913	-0.1060984224	-0.0750539311
44	-0.0314533516	-0.1067063577	-0.0752530061
46	-0.0318432669	-0.1072780356	-0.0754347687
48	-0.0322159188	-0.1078173020	-0.0756013832

Table 2: The one-loop coefficient of the SF coupling $p_{1,1}(L/a, L_s)$ with $L_s = 6$, $am_5 = 1$ and $\theta = \pi/5$. In eq.(39), there are two sources of contributions: DWF and PV, which are shown separately in the table.

$L_s \setminus am_5$	0.7	0.8	0.9	1.0	1.1	1.2	1.3
6	-	-	0.0102(8)	0.0125(9)	0.0145(7)	-	-
8	-	0.0047(4)	0.0074(9)	0.0097(9)	0.0119(9)	0.0135(4)	-
10	0.0004(2)	0.0040(9)	0.0066(9)	0.0090(9)	0.0111(9)	0.0129(9)	0.0135(2)
12	0.0007(9)	0.0037(9)	0.0064(9)	0.0088(9)	0.0108(9)	0.0126(9)	0.0139(8)
16	0.0006(10)	0.0036(9)	0.0063(9)	0.0087(9)	0.0107(9)	0.0125(9)	0.0137(10)

Table 3: The value of A_1 for $L_s = 6, 8, 10, 12, 16$ and $0.7 \leq am_5 \leq 1.3$.

$L/a \setminus L_s$	6	8	10	12	16
4	-0.000602	-0.000518	-0.000527	-0.000538	-0.000545
6	-0.000753	-0.000562	-0.000522	-0.000516	-0.000517
8	-0.000908	-0.000737	-0.000688	-0.000674	-0.000669
10	-0.000825	-0.000695	-0.000655	-0.000643	-0.000637
12	-0.000701	-0.000599	-0.000569	-0.000560	-0.000555
14	-0.000595	-0.000511	-0.000487	-0.000480	-0.000476
16	-0.000512	-0.000439	-0.000419	-0.000413	-0.000411
18	-0.000448	-0.000383	-0.000365	-0.000360	-0.000358
20	-0.000397	-0.000338	-0.000322	-0.000318	-0.000316
22	-0.000356	-0.000302	-0.000288	-0.000284	-0.000282
24	-0.000322	-0.000273	-0.000259	-0.000256	-0.000254

Table 4: The relative deviation $\delta_{1,1}^{(0)}$ with $am_5 = 1$ and $\theta = \pi/5$ for tree level boundary $O(a)$ improvement.

$L/a \setminus L_s$	6	8	10	12	16
4	0.000955	0.000701	0.000597	0.000558	0.000539
6	0.000286	0.000251	0.000227	0.000214	0.000206
8	-0.000129	-0.000128	-0.000126	-0.000127	-0.000127
10	-0.000202	-0.000207	-0.000206	-0.000204	-0.000203
12	-0.000182	-0.000193	-0.000195	-0.000194	-0.000194
14	-0.000150	-0.000162	-0.000166	-0.000166	-0.000166
16	-0.000123	-0.000134	-0.000138	-0.000139	-0.000140
18	-0.000101	-0.000112	-0.000115	-0.000117	-0.000117
20	-0.000085	-0.000094	-0.000098	-0.000099	-0.000099
22	-0.000072	-0.000080	-0.000083	-0.000084	-0.000085
24	-0.000062	-0.000069	-0.000072	-0.000073	-0.000074

Table 5: The relative deviation $\delta_{1,1}^{(1)}$ with $am_5 = 1$ and $\theta = \pi/5$ for one-loop level boundary $O(a)$ improvement.